Optical anisotropy and spontaneous ordering in $Ga_{0.5}In_{0.5}P$: An investigation using reflectance-difference spectroscopy

J. S. Luo, J. M. Olson, Sarah R. Kurtz, D. J. Arent, and K. A. Bertness
National Renewable Energy Laboratory, Golden, Colorado 80401

M. E. Raikh and E. V. Tsiper*
Department of Physics, University of Utah, Salt Lake City, Utah 84112
(Received 1 April 1994; revised manuscript received 24 October 1994)

We have applied reflectance-difference spectroscopy (RDS) to the study of optical anisotropy in spontaneously ordered $Ga_{0.5}In_{0.5}P$ grown by metal-organic chemical-vapor deposition. The degree of order in $Ga_{0.5}In_{0.5}P$ has been associated previously with a shift of the band-gap energy ΔE_0 and a crystal-field valence-band splitting Δ_C. Theoretically, both quantities are, to first order, quadratic functions of the long-range order parameter η, which varies from 0 to 1 for disordered and perfectly ordered $Ga_{0.5}In_{0.5}P$, respectively. The main RD spectral feature in partially ordered $Ga_{0.5}In_{0.5}P$ is a bulk-induced, asymmetric peak at E_0 with a long tail that extends well below E_0 and a sharp high-energy cutoff at $E_0+\Delta_C$. We find experimentally and theoretically that the intensity of this RD spectral feature is proportional to $\sqrt{(\Delta E_0)}$ and, therefore, is linear with the order parameter. This makes RDS particularly useful for measuring the optical anisotropy of high-band-gap $Ga_{0.5}In_{0.5}P$. We also compare heterostructures of GaAs and $Al_{0.5}In_{0.5}P$ on $Ga_{0.5}In_{0.5}P$ with uncoated $Ga_{0.5}In_{0.5}P$ in an effort to separate bulk-, surface-, and interface-induced RD spectral features.

I. INTRODUCTION

Spontaneous ordering in $Ga_{0.5}In_{0.5}P$ (hereafter referred to as GaInP) has attracted considerable attention in recent years.[1–4] The ordered structure is CuPt-like, with alternating {111} planes of $Ga_{0.5+\eta/2}In_{0.5-\eta/2}P$ and $Ga_{0.5-\eta/2}In_{0.5+\eta/2}P$, where η is the long-range order parameter. Perfectly ordered GaInP ($\eta=1$) would be composed of alternating {111} planes of GaP and InP. All GaInP studied to date are only partially ordered ($\eta<1$). Associated with η are changes in the electronic[5–7] and optical properties of GaInP. The effect of ordering on the optical band gap of GaInP includes two major features: (1) experimentally[8] and theoretically[9] the band gap E_0 is reduced, in some cases, depending on the growth conditions, by more than 100 meV,[10–12] and (2) at the Γ point, the fourfold degenerate valence-band maximum for disordered GaInP is split with a crystal-field energy Δ_C.[2] This is illustrated in Fig. 1. Theoretically, the ordering-induced shifts of the band gap[13] (ΔE_0) and Δ_C (Ref. 14) are, to first order, quadratic functions of η. This implies that for samples with weak ordering ($\eta \ll 1$), detection of the ordering in GaInP by traditional optical techniques is difficult. This is consistent with previous experimental work using electroreflectance,[15,16] photoreflectance,[16] photoluminescence[2,17,18] (PL), photoluminescence excitation[17–19] (PLE), and piezomodulated reflectance[20,21] (PZR) spectroscopies to measure ΔE_0 and Δ_C in partially ordered GaInP. For example, Alonso *et al.*[21] found that Δ_C is approximately proportional to ΔE_0 and is approximately 2 meV for a sample with a band gap (at 15 K) of 1.989 eV ($\Delta E_0=0.011$ eV). The maximum observed Δ_C (at 15 K) is 31 meV for $E_0=1.88$ eV ($\Delta E_0=0.12$ eV).

In this paper, we use reflectance-difference spectroscopy (RDS) to examine a number of GaInP structures grown under conditions that yield a wide range of band-gap energies. RDS measures the anisotropy of optical reflectance, and heretofore was used to study the anisotropic surface reconstruction of III-V materials with isotropic bulk properties.[22] For ordered GaInP, bulk anisotropic electronic[5,7] and optical properties were observed previously.[2,17–21] We, therefore, expect RDS to measure both the surface and bulk anisotropic optical features of

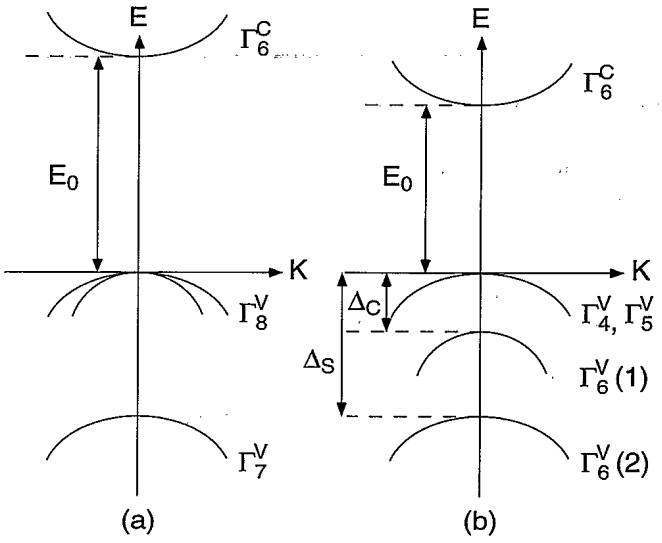

FIG. 1. Γ-point band structure of (a) a random alloy and (b) perfectly ordered GaInP with CuPt structure. The energies are not to scale.

GaInP. In the following sections, we show that the main spectral feature in all samples is a bulk-induced, asymmetric peak at E_0 with a long tail that extends well below E_0 and a sharp high-energy cutoff at $E_0+\Delta_C$. The intensity of this peak varies with $\sqrt{(\Delta E_0)}$. This means that the RDS peak intensity at E_0 is linear with η (presumably, the probe volume average of η). Compared to other optical techniques, RDS is, therefore, particularly useful for detecting small degrees of ordering in GaInP. Additional experiments show that the strong RD spectral features at energies between $E_0+\Delta_S$ and 3.0 eV are probably surface induced, where Δ_S, about 100 meV, is the spin-orbit splitting as shown in Fig. 1. Using the Luttinger model,[23] we also derive an analytical expression that fits well the RD spectral line shape at E_0 and yields the experimentally derived relation between the peak intensity and ΔE_0. Interestingly, the theory shows that the RDS signal at E_0 is sensitive to the anisotropy of the refraction coefficient n_α and not the anisotropy of the extinction coefficient k_α.

II. EXPERIMENTAL DETAILS

A detailed description of RDS techniques and the setup used in this work can be found elsewhere.[22,24] The RD spectrum is measured as $2\times(R_{1\bar{1}0}-R_{110})/(R_{1\bar{1}0}+R_{110})$, where R_{110} and $R_{1\bar{1}0}$ are reflectance of the light polarized along [110] and [1$\bar{1}$0], respectively. All RDS measurements are performed in air at room temperature.

No special sample preparation is performed before the measurement. Most of the samples have been stored in the air for periods of days to months. Immersing the samples in 10% HCl:H_2O solution for 5 min prior to a measurement had virtually no affect on the RD spectrum of a given sample, and the spectrum for a freshly grown sample is essentially the same as that for the old samples. Most of the samples were grown by metal-organic chemical-vapor deposition (MOCVD) using various growth conditions to effect changes in the degree of order and optical properties of the alloy.[25] The general growth information for the MOCVD samples can be found elsewhere.[25] For comparison, we also examined a GaInP sample grown by liquid-phase epitaxy (LPE). This sample has a normal band gap of 1.92 eV at room temperature and exhibits no evidence of ordering.

All samples were grown on vicinal (001) GaAs substrates. The degree of ordering and the optical properties of GaInP are also functions of the substrate tilt or misorientation from the (001) plane.[10,17,18,26] Here, the amount of tilt is denoted as $X°B$, indicating a misorientation of $X°$ from the (001) plane toward the (111)B plane.

III. RESULTS

In Fig. 2(a) we show a typical RD spectrum for samples representative of partially ordered GaInP. The presence of ordering has been verified by transmission electron diffraction. We observe at least four spectral signatures for ordered GaInP samples: (1) a sharp, negative, and asymmetrical peak at the band-gap energy, (2) a broad, positive spectral feature extending from $E_0+\Delta_C$ to approximately 2.2 eV, (3) a negative, but small peak near 2.35 eV, and (4) a negative, broad peak at 3.0 eV. For the disordered LPE sample, all of these features are notably absent, including the sharp peak at E_0 (1.92 eV), and are replaced by a broad negative feature that starts at about 2 eV.

This broad feature of the LPE sample is probably related to the surface roughness,[27] and is also observed in the RD spectrum for two-variant-ordered GaInP as shown in Fig. 2(b). By symmetry, there are four possible variants of CuPt-like ordering. For GaInP grown on singular (001) GaAs, two of the four variants are always observed as a byproduct of an anisotropic surface topography.[28] For thick samples this surface topography efficiently scatters light anisotropically, producing a strong offset, such as that for the 10-μm-thick GaInP of Fig. 2(b). Neither the two-variant ordering, the anisotropic surface topography, nor the strong RDS offset is observed for samples grown on (111)B misoriented substrates.

From Fig. 2, it is reasonable to expect that the RDS intensity at E_0 $(\Delta R/R)_{E_0}$ varies with η in GaInP. Since ΔE_0 is relatively easy to measure and is proportional[13] to η^2, the functional relation between $(\Delta R/R)_{E_0}$ and η can be explored by plotting $(\Delta R/R)_{E_0}$ as a function of ΔE_0, where ΔE_0 is obtained by subtracting the measured band-gap energy from 1.92 eV (the room-temperature

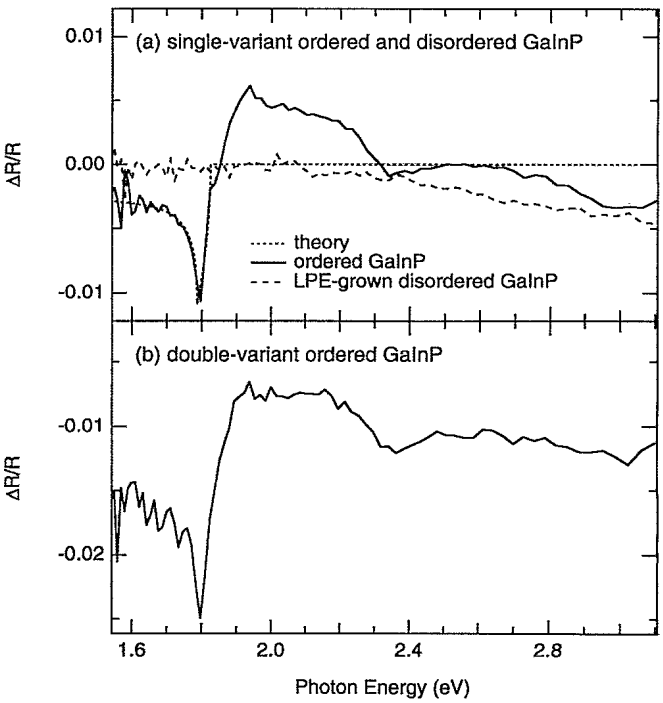

FIG. 2. RD spectra for (a) sample $K316$ with low-band-gap GaInP film and LPE sample with disordered GaInP film, and for (b) sample $K303$ of double-variant-ordered GaInP. Both samples have very similar band-gap energy near 1.80 eV. It is worth noting that the sign for previously published (Ref. 24) RD spectrum of disordered LPE GaInP is wrong due to insufficient knowledge of differentiating cleavage directions. We have obtained new samples and the new experiments support the sign presented here.

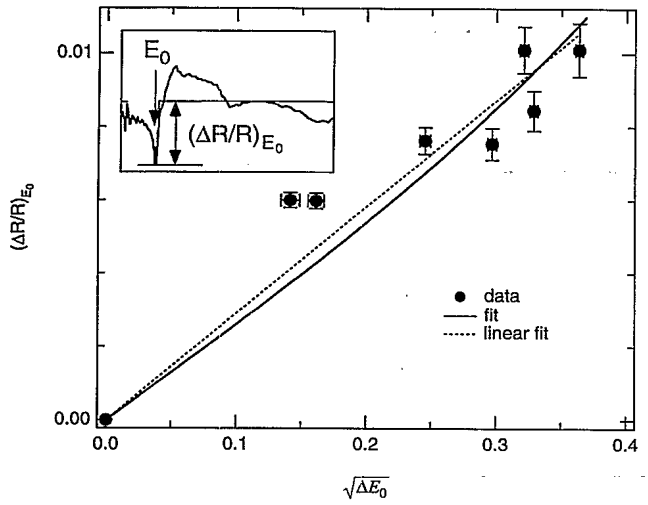

FIG. 3. Plot of RDS intensity at E_0 vs $\sqrt{\Delta E_0}$. Solid dots are measured data, the solid line is a fit using Eq. (22) and $c=(0.19\pm0.01)$ $(\mathrm{eV})^{3/2}$ assuming that both ΔE_0 and ΔE_C are proportional to η^2; we estimate $\Delta E_C=(30\pm3)$ meV for $\Delta E_0=120$ meV from a measurement by Alonso *et al.* (Ref. 21), and the dotted line is a simple linear fit going through the zero point.

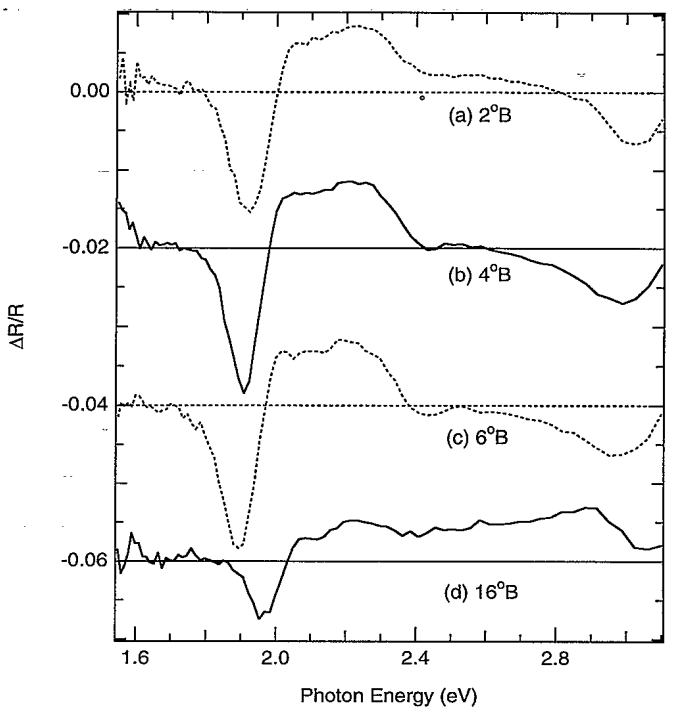

FIG. 4. RD spectra for four GaInP layers ($K535$) grown simultaneously on (a) $2°B$, (b) $4°B$, (c) $6°B$, and (d) $16°B$ substrates. The ordinate of the RDS spectra in (b), (c), and (d) are offset by -2, -4, and -6×10^{-2}, respectively.

band-gap energy for disordered GaInP). Doing so for a series of samples, we find that measured $(\Delta R/R)_{E_0}$ is approximately linear with $\sqrt{(\Delta E_0)}$ (or η), as shown in Fig. 3. Later, we will show that essentially the same result is also obtained from our theoretical calculation, which is illustrated as a solid line in Fig. 3. This result is particularly important when η is very small. When $\eta \ll 1$, the magnitudes of ΔE_0 and Δ_C, which are both roughly proportional to η^2, become comparable to the measurement uncertainty. To distinguish disordered from weakly ordered GaInP, we find that RDS is consistently more reliable than techniques that measure ΔE_0 and Δ_C.

Heretofore, the detection of ordering in an alloy from a measurement of ΔE_0 also required a measurement of the composition that is most accurately accomplished using double-crystal x-ray diffraction to measure the lattice constant of GaInP relative to the closely lattice-matched underlying GaAs substrate. For strain-relaxed, nonlattice-matched materials systems, one must rely on compositional measurement techniques, which are less accurate. However, $(\Delta R/R)_{E_0}$ should be relatively independent of the composition and should, therefore, be useful for studying ordering-related effects in samples where uncertainties in the composition may confound the results. This aspect of the technique is illustrated in Fig. 4, which shows the RDS spectra for a group of four 300-Å-thick GaInP samples ($K535$) grown simultaneously on four different substrates: $2°B$, $4°B$, $6°B$, and $16°B$. Because the growth times for these thin samples are comparable to the time constant of the initial growth transient, the composition of these thin layers is probably different from that of thicker layers grown under steady-state conditions. Also, the composition of these very thin samples cannot be accurately measured with double-crystal x-ray diffraction. Using PL, PLE, or PZR on thicker samples, we typically see the band gap decrease from 1.85 eV for the $2°B$ sample to 1.82 eV for the $4°B$ and $6°B$ samples, and then increase to 1.88 eV for the $16°B$ layer. A similar E_0 shift with substrate tilt is seen for the four samples of Fig. 4 but all of the spectral features are blue shifted about 90 meV. Furthermore, the overall RDS spectral line shapes of these 300-Å-thick GaInP layers are similar to that of the 10-μm-thick, lattice-matched GaInP layers, as shown in Fig. 2(a).

For sample thicknesses between 0.1 and 6 μm, the RDS spectrum of *ordered* GaInP is modulated by interference effects, as shown in Fig. 5, where we illustrate the RD spectra of a 2-μm-thick sample [Fig. 5(a)] and a 0.5-μm-thick sample [Fig. 5(b)]. Both samples were grown under conditions similar to those used for $K316$ [Fig. 2(a)] and designed to yield a partially ordered alloy with a room-temperature band gap of about 1.85 eV. Interference fringes are clearly seen in both spectra. These fringes are caused by a refractive index anisotropy Δn_α. For the 2-μm-thick sample, the interference fringes oscillate rapidly for $E<E_0$ (extinction coefficient $k_\alpha=0$) and damp quickly for $E>E_0$ ($k_\alpha>0$). Compared to the thick sample, the first interference fringe of the 0.5-μm-thick samples appears at higher energy and the oscillations damp more slowly, as expected. The spectral features that are not masked by interference effects (those above 2.0 eV for the 2-μm-thick sample and above 2.4 eV for the 0.5-μm-thick sample) are essentially the same as that of the 10-μm-thick sample ($K316$) of Fig. 2(a).

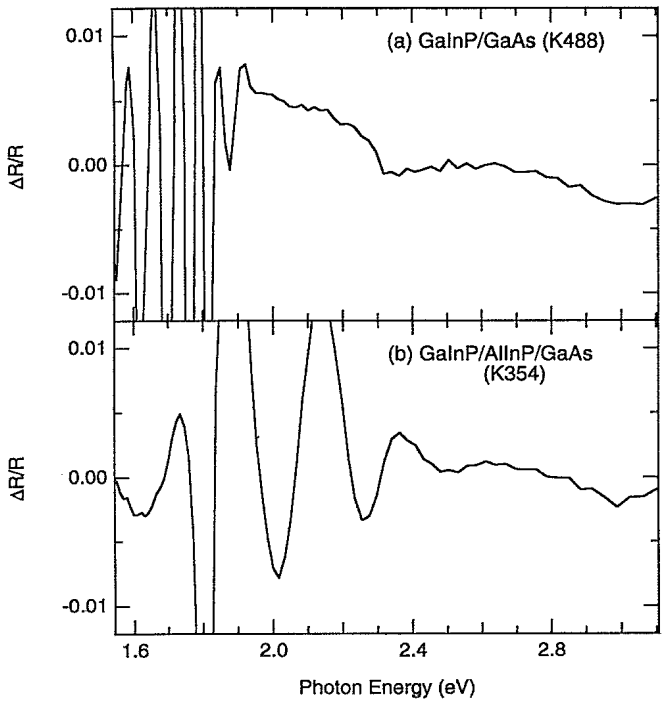

FIG. 5. RD spectra for (a) a 2-μm-thick GaInP sample ($K488$) on a 4°B GaAs substrate, and (b) a 0.5-μm-thick GaInP sample ($K354$) on a 2°B substrate.

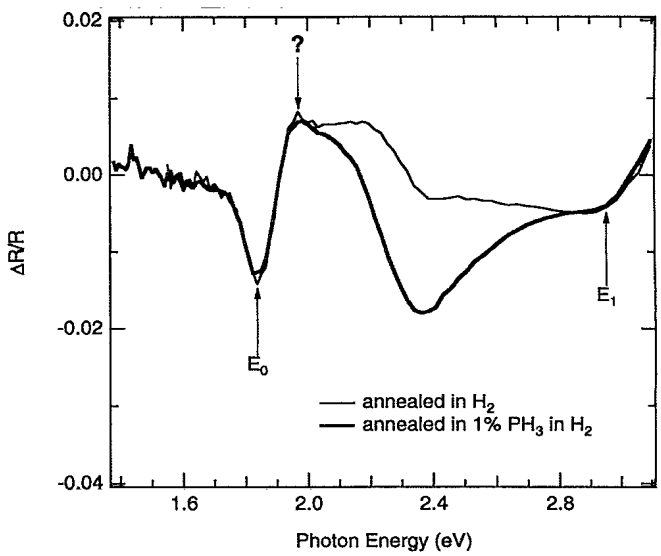

FIG. 6. *In situ* RD spectra measured at 85 °C (Ref. 24).

IV. DISCUSSIONS

A. RDS peak assignment

From previous work it is reasonable to expect that GaInP should exhibit both bulk- and surface-induced RD features, and indeed, the RD spectrum of GaInP is significantly richer than that of GaAs. The problem, now, is to decipher the spectra of Figs. 2 and 4. We recently published one approach to this problem.[24] We compared *in situ* the RDS spectra of H_2- and PH_3-annealed GaInP. A summary of this work is shown in Fig. 6. The annealing times (temperatures) were short (low) compared to those required to effect changes in the bulk of the GaInP. On the other hand, the annealing atmosphere should have a definite effect on the surface structure with PH_3 stabilizing a surface structure composed probably of P dimers and H_2 producing a group-III terminated surface. Spectral features affected or unaffected by these annealing conditions were then classified as surface- or bulk-induced, respectively. In Fig. 6, the bulk features were assigned to E_0 and E_1. The peak at E_0 is caused by the ordering-induced splitting of the valence-band maximum, and a theoretical model for E_0 is presented in the next section. (We have also developed a model for E_1, which shows that the peak at 3.0 eV is induced by the effect of bandfoldings associated with the E_1 critical point, details to be published). The theoretical model for E_0 has a sharp cutoff at $E_0+\Delta_C$ and does not fit well the positive RDS peak on the high-energy side of E_0. This positive peak is not affected by a PH_3 anneal, implying that it is bulk induced.[24] However, we also noted that this peak disappears reversibly at high temperatures,[24] something that does not happen to the E_0 and E_1 peaks. This would imply that this positive peak is induced by a near surface structure (such as strain) immune to the state of the surface but not present at high temperatures. The remainder of the positive plateau is strongly influenced by the state of the surface.

There is evidence in the literature to suggest that the small negative peak at 2.35 eV could be a bulk-induced folded L-band state first observed by Kurtz.[29] However, this peak is strongly enhanced for samples annealed in PH_3, and the sign and strength of this peak are consistent with a phosphorus-stabilized surface reconstruction consisting of P dimer bonds aligned with $[1\bar{1}0]$. In the H_2-annealed (or air exposed) state, the residual peak at 2.35 eV could be due either to the bulk-induced folded L band or residual P surface dimers.

To shed more light on this problem, we use one other approach modifying the surface of the GaInP: we produce *surface-free* GaInP by coating it with optically thin, lattice-matched layers of either GaAs or $Al_{0.5}In_{0.5}P$ (hereafter AlInP). For reference, the RDS signatures of these two materials are shown in Fig. 7. The overlayers were grown in the same MOCVD reactor using conditions similar to those used for the growth of the GaInP layers. Note first that the *ex situ* RDS spectrum of GaAs is small relative to that measured for GaInP. Second, the RDS spectrum of AlInP exhibits a distinct negative peak near its direct band edge as expected from TEM studies of AlInP.[30] However, below this peak ($E<2.5$ eV), the RDS signal is essentially zero. Using these two layers, we prepared a set of samples comprised of a 300-Å-thick GaInP layer coated with either a 200-Å-thick GaAs or AlInP layer. Each structure was grown simultaneously on 4°B and 16°B GaAs substrates using MOCVD growth conditions identical to those used for Figs. 2(a) and 4.

The RD spectra of the coated GaInP layers are shown

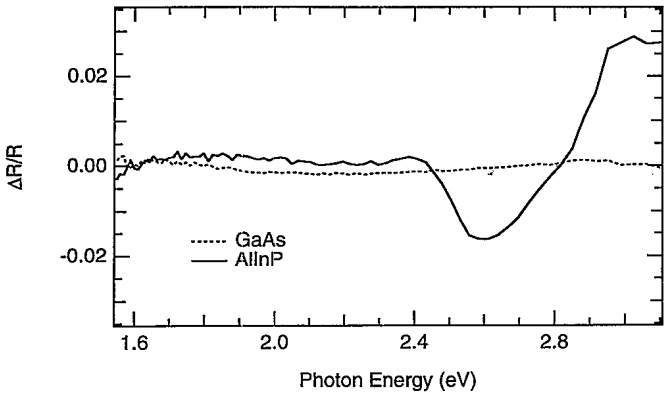

FIG. 7. RD spectra for GaAs (dashed line) and AlInP (solid line) grown by MOCVD on GaAs.

in Fig. 8. Comparing Fig. 8(a) with Figs. 8(b) and 8(c), we make the following observations.

(i) The bulk-induced peaks at E_0 and E_1 are largely unaffected by the coatings. The E_0 peak intensity ratios of the 4°B sample to 16°B sample $(\Delta R/R)|_{E_0}^{4°B}/(\Delta R/R)|_{E_0}^{16°B}$ for uncoated, GaAs-coated, and AlInP-coated GaInP (2.1, 1.7, and 1.8, respectively) are all within 25% of each other. There also appears to be a systematic baseline shift for the coated 4°B samples in the vicinity of the E_0 peak.

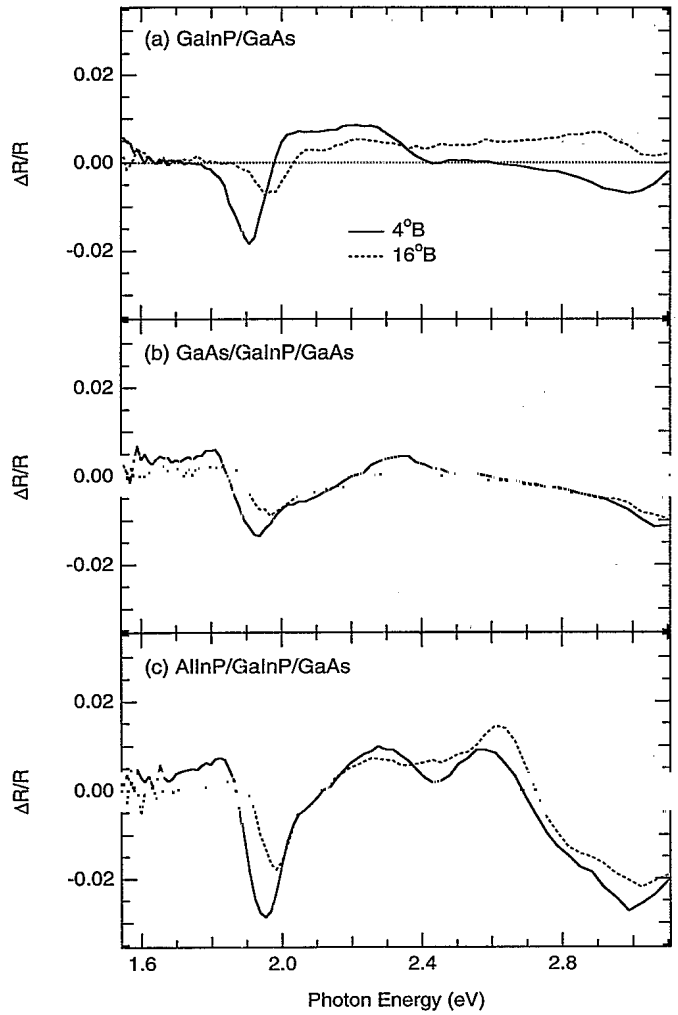

FIG. 8. RD spectra of (a) GaInP, (b) GaAs-coated GaInP, and (c) AlInP-coated GaInP grown on 4° B and 16° B GaAs substrates.

(ii) The broad positive plateau between $E_0+\Delta_C$ and 2.3 eV seen in Figs. 2(a) and 8(a), part of which is supposedly bulk induced, now appears as a negative shoulder on the high-energy side of the E_0 peak for both the GaAs- and AlInP-coated samples.

(iii) The peak at 2.35 eV effectively disappears for the GaAs-coated 4°B sample.

(iv) Whereas the RD spectral line shapes of the two uncoated GaInP samples depend strongly on the measured ΔE_0, the line shapes of the coated samples depend predominantly on the coating material and not on ΔE_0.

These observations and those of our previous *in situ* study lead one to conclude that the broad positive plateau between $E_0+\Delta_C$ and 2.3 eV is surface induced. The presence of the GaAs or AlInP overlayer effectively precludes formation of P or group-III dimers, thereby quenching the peak at 2.35 eV and any other surface reconstruction related features. The quenching of the low-energy portion of the broad positive feature lends support to the idea that this feature is due to some subsurface (yet surface-induced) structure (e.g., strain) that is relieved in the surface-free coated samples. Presently there is no evidence of a bulk-induced peak at 2.35 eV. Considering the size of this peak in electroreflectance or photoreflectance studies, it is possible that it is simply buried in the noise. Better signal-to-noise and more ordered samples may help clarify this problem.

While the GaAs and AlInP coatings eliminate the surface effects, they introduce a second interface, the symmetry and RDS properties of which have not been studied to date. Therefore, we still cannot draw any definitive conclusions about the pronounced, negative signal that extends 300–400 meV beyond the high-energy side of E_0 for the coated GaInP samples. However, since the intensity but not the shape of this feature scales with the degree of order (or ΔE_0), one is inclined to conclude that it is bulk induced. We shall see, however, in the next section that the peak at E_0 should cut off sharply to zero at $E_0+\Delta_C$ for weakly ordered samples. Strongly ordered samples may include a contribution from the spin-orbit band. However, this should simply extend the zero cut off to $E_0+\Delta_S$, where Δ_S is at most 120 meV. Further experiments are needed to clarify this problem.

B. Theory

In this section, we derive an analytical expression for the RDS feature near E_0. Essentially, we calculate the reflectance difference for the light polarized along [110] and [1$\bar{1}$0] as a function of energy for a material exhibiting an anisotropic splitting Δ_C of the valence-band maximum. The reflectance of light with polarization α can be expressed in terms of the coefficients of refraction n_α and extinction k_α as

$$R_\alpha=\frac{(n_\alpha-1)^2+k_\alpha^2}{(n_\alpha+1)^2+k_\alpha^2} . \quad (1)$$

In a cubic crystal, there is no polarization dependence of the optical coefficients. Ordering reduces the cubic symmetry, thus allowing for the optical anisotropy. The major manifestation of the reduced symmetry is the splitting of the valence-band maximum. Since the absorption from each of the splitted branches of the valence-band spectrum (heavy and light holes) is sensitive to the polarization of light, the optical anisotropy is expected in the vicinity of $E<E_0+\Delta_C$, for a small value of Δ_C.

Calculating reflectance as the function of photon energy thus requires information of the anisotropic valence-band spectra and the corresponding wave functions, which are then used for calculating k_α:

$$k_\alpha(\omega)=\frac{2\pi^2e^2}{m_0^2n_0\omega^2}\sum_{\mu\mathbf{K}}|M^\alpha_{\mu\mathbf{K}}|^2\delta[\hbar\omega-(E^c_{\mathbf{K}}-E^v_{\mu\mathbf{K}})] . \quad (2)$$

Here ω is the frequency of light; $E^c_{\mathbf{K}}$ and $E^v_{\mu\mathbf{K}}$ are energies of the conduction and valence bands; m_0 is the free-electron mass; n_0 is the refraction index in the absence of ordering; index $\mu=\{l_1,l_2,h_1,h_2\}$ numerates two pairs, "l" as light holes and "h" as heavy holes, of the valence bands; and $M^\alpha_{\mu\mathbf{K}}$ stands for the matrix element for the momentum operator projected along α direction, $P_\alpha=-i\hbar\partial/\partial x_\alpha$, taken between the wave functions of the conduction and valence bands. Note that the branches of the valence bands are degenerate in pairs: $E^v_{h_1\mathbf{K}}=E^v_{h_2\mathbf{K}}$ and $E^v_{l_1\mathbf{K}}=E^v_{l_2\mathbf{K}}$. The refraction coefficient n_α can be found from Eq. (2) using the Kramers-Kronig relations.

Equation (2) can be expressed through the Bloch amplitudes of the conduction and valence bands u^c and $u^v_{\mu\mathbf{K}}$, respectively.

$$\begin{aligned}k_\alpha(\omega)&=\frac{2\pi^2e^2}{m_0^2n_0\omega^2}\sum_{\mu\mathbf{K}}\langle u^c|P_\alpha|u^v_{\mu\mathbf{K}}\rangle\langle u^v_{\mu\mathbf{K}}|P_\alpha|u^c\rangle \\ &\quad\times\delta[\hbar\omega-(E^c_{\mathbf{K}}-E^v_{\mu\mathbf{K}})] \\ &=\frac{2\pi^2e^2}{m_0^2n_0\omega^2}\langle u^c|P_\alpha\mathbf{J}(\omega)P_\alpha|u^c\rangle , \end{aligned} \quad (3)$$

where we have introduced the operator $\mathbf{J}(\omega)$ defined as

$$\mathbf{J}(\omega)=\sum_{\mu\mathbf{K}}|u^v_{\mu\mathbf{K}}\rangle\langle u^v_{\mu\mathbf{K}}|\delta[\hbar\omega-(E^c_{\mathbf{K}}-E^v_{\mu\mathbf{K}})] . \quad (4)$$

Thus, our goal is to calculate $\mathbf{J}(\omega)$ in the presence of ordering. Our calculation is in the framework of the standard Luttinger model,[23] which is commonly used to describe the valence-band structure of wide-band-gap materials. The basis used in the calculation is

$$\begin{aligned}h_\uparrow&=\frac{1}{\sqrt{2}}|(X+iY)\uparrow\rangle , \\ l_\uparrow&=-\sqrt{\tfrac{2}{3}}|Z\uparrow\rangle+\frac{1}{\sqrt{6}}|(X+iY)\downarrow\rangle , \\ l_\downarrow&=-\sqrt{\tfrac{2}{3}}|Z\downarrow\rangle-\frac{1}{\sqrt{6}}|(X-iY)\uparrow\rangle , \\ h_\downarrow&=\frac{1}{\sqrt{2}}|(X-iY)\downarrow\rangle , \end{aligned} \quad (5)$$

where X, Y, and Z denote the periodic Bloch functions of p type, and $\uparrow$ and $\downarrow$ are spin-up and -down states, respectively.

In the calculation, we adopt the spherical approximation, which neglects the effects caused by the cubic symmetry of the crystal. Obviously, within the spherical approximation, the symmetry of the ordering-induced perturbation is axial. Thus, we can choose the z axis as the ordering direction. We also assume that there is no ordering-induced coupling with the spin-orbit-split-off band. This should be accurate in the limit $(\Delta_C/\Delta_S)^2\ll1$ for $\eta\ll1$. Perturbation caused by ordering is diagonal in the basis shown in Eq. (5). Such diagonal matrix elements of the perturbation are equal in pairs: $(h_\uparrow\Delta\mathbf{H}h_\uparrow)\equiv(h_\downarrow\Delta\mathbf{H}h_\downarrow)$ and $(l_\uparrow\Delta\mathbf{H}l_\uparrow)\equiv(l_\downarrow\Delta\mathbf{H}l_\downarrow)$, where $\Delta\mathbf{H}$ is the perturbation. If the energy of the heavy-hole band at the Γ point is chosen as a reference, the matrix of the Hamiltonian can be written as

$$\mathbf{H}=\begin{bmatrix} F & B & C & 0 \\ B^* & G & 0 & -C \\ C^* & 0 & G & B \\ 0 & -C^* & B^* & F \end{bmatrix} , \quad (6)$$

with the parameters F, G, B, and C given by

$$F=-(\gamma_1-2\gamma_2)\frac{\hbar^2K_z^2}{2m_0}-(\gamma_1+\gamma_2)\frac{\hbar^2(K_x^2+K_y^2)}{2m_0} , \quad (7a)$$

$$G=-(\gamma_1+2\gamma_2)\frac{\hbar^2K_z^2}{2m_0}-(\gamma_1-\gamma_2)\frac{\hbar^2(K_x^2+K_y^2)}{2m_0}-\Delta_C , \quad (7b)$$

$$B=2\sqrt{3}\gamma_2\frac{\hbar^2K_z(K_x-iK_y)}{2m_0} , \quad (7c)$$

$$C=\sqrt{3}\gamma_2\frac{\hbar^2(K_x-iK_y)^2}{2m_0} , \quad (7d)$$

where γ_1 and γ_2 are the Luttinger parameters.[23] In addition to the standard Luttinger matrix, the element G contains an ordering-related term $-\Delta_C$, which is proportional to the square of the order parameter η when $(\Delta_C/\Delta_S)^2\ll1$.[31] The reason why Δ_C is proportional to η^2 is the following: Ordering couples the states from the top of the valence band with the corresponding states of the L extrema along the ordering axis. The coupling between the states of the valence-band maximum appears only in the second order in η. It is obvious, also, that the eigenvalues of the matrix (6) are doubly degenerate even in the presence of ordering.

Next, we can express $\mathbf{J}(\omega)$ in terms of $\mathbf{H}$. From Eq. (4), $\mathbf{J}(\omega)$ can be written as the imaginary part of the Green's function

$$\mathbf{J}(\omega)=\frac{1}{\pi}\,\mathrm{Im}\sum_{\mathbf{K}}\frac{1}{\mathbf{H}-E^c_{\mathbf{K}}+\hbar\omega-i\delta} , \quad (8)$$

where δ is infinitesimally small and positive. $\mathbf{J}(\omega)$ in Eq. (8) can then be obtained by calculating the inverse matrix of $\mathbf{H}-E^c_{\mathbf{K}}+\hbar\omega$. Consequently, we calculate $(\mathbf{H}-E)^{-1}$ as

$$(\mathbf{H}-E)^{-1}=\frac{1}{\Delta(E)}\begin{bmatrix} G-E & -B & -C & 0 \\ -B^* & F-E & 0 & C \\ -C^* & 0 & F-E & -B \\ 0 & C^* & -B^* & G-E \end{bmatrix}, \quad (9)$$

where $\Delta(E)$ is defined as

$$\Delta(E)=(F-E)(G-E)-|B|^2-|C|^2 . \quad (10)$$

It is seen that the matrix $(\mathbf{H}-E)^{-1}$ has the same structure as the matrix $(\mathbf{H}-E)$. In addition, the off-diagonal matrix elements obey the relation $(\mathbf{H}-E)^{-1}_{ij}=-(\mathbf{H}-E)_{ij}/\Delta(E)$. The determinant of $(\mathbf{H}-E)$ is equal to Δ^2. The energy spectra of the valence bands determined from $\Delta(E)=0$ can be written as

$$E^v_{h\mathbf{K},l\mathbf{K}}=\frac{F+G}{2}\pm\left[\left[\frac{F-G}{2}\right]^2+|B|^2+|C|^2\right]^{1/2} . \quad (11)$$

In Eq. (11), the plus and minus signs are for heavy and light holes, respectively. Substituting Eqs. (7) into (11), we obtain the dispersion relation for the heavy- and light-hole branches, depending on the polar angle $\theta_{\mathbf{K}}$ of the vector $\mathbf{K}$:

$$E_{h\mathbf{K},l\mathbf{K}}=-\frac{\Delta_C}{2}-\gamma_1\frac{\hbar^2K^2}{2m_0} \pm\left[\left[\frac{\Delta_C}{2}-2\gamma_2\frac{\hbar^2K^2}{2m_0}\right]^2+3\Delta_C\gamma_2\frac{\hbar^2K^2}{2m_0}\sin^2\theta_{\mathbf{K}}\right]^{1/2} . \quad (12)$$

The operator $\mathbf{J}(\omega)$ must be diagonal in the basis Eq. (5) because of the axial symmetry. Essentially the off-diagonal elements of the matrix in Eq. (9) vanish after the summation over the azimuth angle of the vector $\mathbf{K}$ in Eq. (8). The imaginary part of the diagonal elements of the matrix $(\mathbf{H}-E^c_{\mathbf{K}}+\hbar\omega)^{-1}$ results from the poles, which correspond to the energies $E=E^c_{\mathbf{K}}-\hbar\omega$ at which $\Delta(E)=0$. Consequently, we obtain

$$\mathbf{J}(\omega)=\begin{bmatrix} P(\omega) & 0 & 0 & 0 \\ 0 & Q(\omega) & 0 & 0 \\ 0 & 0 & Q(\omega) & 0 \\ 0 & 0 & 0 & P(\omega) \end{bmatrix}, \quad (13)$$

where

$$P(\omega)=\sum_{\mathbf{K}}\frac{\hbar\omega-E^c_{\mathbf{K}}+G}{2(\hbar\omega-E^c_{\mathbf{K}})+F+G}\{\delta[\hbar\omega-(E^c_{\mathbf{K}}-E^v_{h\mathbf{K}})] +\delta[\hbar\omega-(E^c_{\mathbf{K}}-E^v_{l\mathbf{K}})]\} , \quad (14a)$$

$$Q(\omega)=\sum_{\mathbf{K}}\frac{\hbar\omega-E^c_{\mathbf{K}}+F}{2(\hbar\omega-E^c_{\mathbf{K}})+F+G}\{\delta[\hbar\omega-(E^c_{\mathbf{K}}-E^v_{h\mathbf{K}})] +\delta[\hbar\omega-(E^c_{\mathbf{K}}-E^v_{l\mathbf{K}})]\} . \quad (14b)$$

Substituting Eqs. (13) and (14) into Eq. (3) and using the basis in Eq. (5), we calculate $k(\omega)$:

$$k_\alpha(\omega)=\frac{2\pi^2e^2}{m_0^2n_0\omega^2}p_{cv}^2\{\tfrac{4}{3}Q(\omega)+\sin^2\theta_\alpha[P(\omega)-Q(\omega)]\} , \quad (15)$$

where p_{cv} is the Kane matrix element, and θ_α is the angle between the polarization of light and the ordering axis. The factor $\frac{4}{3}$ originates from the coefficient $\sqrt{(2/3)}$ in the z component of light-hole wave functions [see Eq. (5)].

Calculations of the functions $P(\omega)$ and $Q(\omega)$ can be found in the Appendix. In Fig. 9, we plot the two functions for different values of μ, where

$$\mu=\frac{\gamma_0+\gamma_1}{\gamma_2}=2\frac{m_h+m_l}{m_h-m_l}+4\frac{m_hm_l}{m_e(m_h-m_l)} . \quad (16)$$

Here, m_h, m_l, and m_e are the effective masses of heavy holes, light holes, and electrons, respectively, for a disordered sample, and $\gamma_0=(m_0/m_e)$. Generally, for the usual relation between the effective masses $m_h>m_l\geq m_e$, μ is greater than six. Figure 6 shows clearly that $P(\omega)$ and $Q(\omega)$ are not very sensitive to μ for $\mu\geq 6$. In the limit of large μ, $P(\omega)$ and $Q(\omega)$ can be expressed as

$$P(\omega)=\frac{(2m^*)^{3/2}}{4\pi^2\hbar^3}\sqrt{\hbar\omega-E_0} , \quad (17a)$$

$$Q(\omega)=\frac{(2m^*)^{3/2}}{4\pi^2\hbar^3}\sqrt{\hbar\omega-E_0-\Delta_C} . \quad (17b)$$

Each of the square roots in Eq. (17) is assumed to be zero when the argument is negative. The effective mass m^* in Eq. (17) is chosen in such a way that these equations are exact for $\hbar\omega-E_0\gg\Delta_C$:

$$m^*=\left[\tfrac{1}{2}\left[\frac{m_em_l}{m_e+m_l}\right]^{3/2}+\tfrac{1}{2}\left[\frac{m_em_h}{m_e+m_h}\right]^{3/2}\right]^{2/3} . \quad (18)$$

Substituting Eq. (17) into Eq. (15) and using the

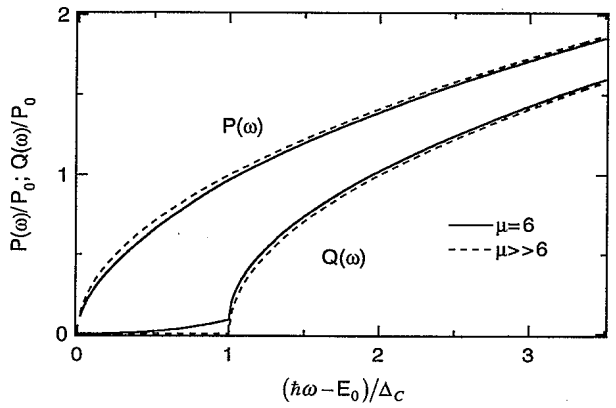

FIG. 9. Plot of normalized $P(\omega)$ and $Q(\omega)$ with different values of μ vs photon energy. See text for the definition of μ and P_0 is $P(\omega)$ at $\hbar\omega=E_0+\Delta_C$ for $\mu\gg 6$.

Kramers-Kronig relations, we calculate $k(\omega)$ and $n(\omega)$:

$$k_\alpha(\omega)=\frac{\beta}{(\hbar\omega)^2}[\tfrac{4}{3}\sqrt{\hbar\omega-E_0-\Delta_C} +\sin^2\theta_\alpha(\sqrt{\hbar\omega-E_0}-\sqrt{\hbar\omega-E_0-\Delta_C})] , \tag{19a}$$

$$n_\alpha(\omega)=n_0-\frac{\beta}{(\hbar\omega)^2}[\tfrac{4}{3}\sqrt{E_0+\Delta_C-\hbar\omega} +\sin^2\theta_\alpha(\sqrt{E_0-\hbar\omega} -\sqrt{E_0+\Delta_C-\hbar\omega})] , \tag{19b}$$

where

$$\beta=\frac{e^2(2m^*)^{3/2}}{2\hbar m_0^2 n_0}p_{cv}^2 .$$

For any realistic values of parameters, we should have $|n(\omega)-n_0|\ll n_0$. Then the first differential of Eq. (1) can be simplified to

$$\Delta R(\omega)=R(n+\Delta n,k+\Delta k) -R(n,k)\approx 4\frac{(n_0-1)}{(n_0+1)^3}\Delta n(\omega) , \tag{20}$$

where $\Delta n(\omega)=n_{1\bar{1}0}-n_{110}$ and $\Delta k(\omega)=k_{1\bar{1}0}-k_{110}$. In deriving Eq. (20), we neglected terms proportional to $k^2(\omega)$ because $k(\omega)$ is of the order of $|n(\omega)-n_0|$.

The values of $\sin^2\theta_\alpha$ between each of the directions [110], [$1\bar{1}0$], and the ordering axis [$1\bar{1}1$] are 1 and $\frac{1}{3}$, respectively. With Eqs. (19) and (20), we then obtain RDS intensity as the function of photon energy

$$\frac{\Delta R}{R}=-\frac{c}{(\hbar\omega)^2}(\sqrt{\Delta_C+E_0-\hbar\omega}-\sqrt{E_0-\hbar\omega}) . \tag{21}$$

Here $c=8\beta/3(n_0^2-1)$.

Equations (20) and (21) account for most of the bulk physical effects described in the previous section. According to Eq. (21), the RDS peak occurs at $\hbar\omega=E_0$ and is given by

$$\left[\frac{\Delta R}{R}\right]_{E_0}=-\frac{c}{E_0^2}\sqrt{\Delta_C} . \tag{22}$$

Since Δ_C is proportional to ΔE_0, Eq. (21) is equivalent to the experimental result of Fig. 3.

The line shape of Eq. (21) is shown as a dotted line in Fig. 2(a). The fitted value c is (0.19 ± 0.01) $(\text{eV})^{3/2}$. We can also estimate the value of c theoretically using $n_0=3.3\pm0.2$,[32,33] $m^*\approx(0.8m_e)$, where $m_e\approx0.09m_0$,[34] and $[2p_{cv}^2/m_0]=26$ eV estimated[34] from the values for GaP (Ref. 35) and InP.[36] The calculated value of c is (0.15 ± 0.01) $(\text{eV})^{3/2}$. The discrepancy between the experimentally derived and the calculated values of c is probably associated with the uncertainty of $[2p_{cv}^2/m_0]$ for ordered GaInP. Essentially, we are not certain how the effect of bandfoldings resulting from the ordering affects the value of $[2p_{cv}^2/m_0]$. It is worth noting that the values of p_{cv}^2 and m^* used in previous work[24] are factors approximately three larger and two smaller, respectively, than that used here, but yield a similar value for c. Details of estimated parameters aside, a comparison of theoretical and experimental RDS line shapes is a better measure of the goodness of fit. While it is not meant to treat the apparently complex behavior seen at energies greater than $E_0+\Delta_C$, this theory fits well the experimental line shape at E_0 and reproduces the pronounced subband-gap tail observed in the RD spectra of low-band-gap samples such as those presented in Fig. 2. The tail below E_0 is a direct result of Eq. (19), which shows that the bulk RDS signal is sensitive to $\Delta n(\omega)=n_{1\bar{1}0}-n_{110}$ as opposed to $\Delta k(\omega)$. This is also consistent with the interference oscillations observed for samples of intermediate thickness as shown in Fig. 5. In either case no subband-gap signals would be expected if ΔR were sensitive only to $\Delta k(\omega)$.

V. CONCLUSION

We have demonstrated that RDS is a useful nondestructive technique for studying ordering in semiconductor alloys. For ordered GaInP, RDS signatures at E_0 and E_1 are directly related to the ordering-induced bulk anisotropy. For the RDS feature at E_0, we observe that the peak intensity is proportional to η. This makes RDS particularly useful for studying samples for which η is small. We also present a detailed theory, based upon the Luttinger model, for the RDS feature at E_0. This theory fits well the RDS line shape around E_0 and yields the liner dependence between the peak intensity and η observed experimentally. Interestingly, the theory indicates that the RDS signal at E_0 is caused only by a refraction coefficient n_α anisotropy. We also compare RD spectra of surface-free GaAs and AlInP on GaInP heterostructures with our previously published *in situ* RDS measurements of uncoated GaInP. This way, we are able to determine that the high-energy (between $E_0+\Delta_C$ and E_1) RDS features of uncoated GaInP are mostly surface induced.

ACKNOWLEDGMENTS

We would like to thank Gary Giust for helping us set up the RDS system, Sverre Froyen for helpful conversations, and Su-Huai Wei for pointing out mistakes made on the units of the parameter c and the estimated value for p_{cv}^2 in our previous work.[24] We are also grateful to M. C. Wu, National Tsing Hua University, Hsinchu, Taiwan, for the LPE-grown GaInP sample. This work is supported by the U.S. Department of Energy, Office of Energy Research, Basic Energy Sciences.

APPENDIX

Here we derive $P(\omega)$ and $Q(\omega)$. It is easy to see that the sum $P(\omega)+Q(\omega)$ is just equal to the joint density of

states $g(\omega)$

$$g(\omega)=\sum_{\mathbf{K}}[\delta(\hbar\omega-(E^c_{\mathbf{K}}-E^v_{h\mathbf{K}}))+\delta(\hbar\omega-(E^c_{\mathbf{K}}-E^v_{l\mathbf{K}}))]\ . \tag{A1}$$

It is also convenient to introduce the difference $\chi(\omega)=P(\omega)-Q(\omega)$, which has the form

$$\chi(\omega)=\sum_{\mathbf{K}}\frac{G-F}{2(\hbar\omega-E^c_{\mathbf{K}})+F+G}[\delta(\hbar\omega-(E^c_{\mathbf{K}}-E^v_{h\mathbf{K}}))+\delta(\hbar\omega-(E^c_{\mathbf{K}}-E^v_{l\mathbf{K}}))]\ . \tag{A2}$$

It is helpful to use the relation $\delta(x-a)+\delta(x-b)=|a-b|\delta[(x-a)(x-b)]$. Applied to Eqs. (A1) and (A2), it gives

$$\begin{aligned}\delta(\hbar\omega-(E^c_{\mathbf{K}}-E^v_{h\mathbf{K}}))+\delta(\hbar\omega-(E^c_{\mathbf{K}}-E^v_{l\mathbf{K}}))&=(E^v_{h\mathbf{K}}-E^v_{l\mathbf{K}})\delta[(\hbar\omega-(E^c_{\mathbf{K}}-E^v_{h\mathbf{K}}))(\hbar\omega-(E^c_{\mathbf{K}}-E^v_{l\mathbf{K}}))]\\&=(E^v_{h\mathbf{K}}-E^v_{l\mathbf{K}})\delta(\Delta(E^c_{\mathbf{K}}-\hbar\omega))\ ,\end{aligned} \tag{A3}$$

where the function $\Delta(E)$ is determined by Eq. (10). We have used the fact that $E^v_{h\mathbf{K}}$ and $E^v_{l\mathbf{K}}$ are roots of $\Delta(E)$, so that $\Delta(E)=(E-E^v_{h\mathbf{K}})(E-E^v_{l\mathbf{K}})$. Using Eqs. (7), $\Delta(E)$ can be written in the following form:

$$\Delta(E)=\Delta_C^2[\xi(E,\mathbf{K})+3x\sin^2\vartheta]\ , \tag{A4}$$

where

$$\xi(E,\mathbf{K})=\frac{1}{\Delta_C^2}\left[E+\frac{\hbar^2}{2m_0}(\gamma_1-2\gamma_2)K^2\right]\times\left[E+\frac{\hbar^2}{2m_0}(\gamma_1+2\gamma_2)K^2+\Delta_C\right]\ , \tag{A5a}$$

$$x=\gamma_2\frac{\hbar^2K^2}{2m_0\Delta_C}\ . \tag{A5b}$$

Using the expression for the energy spectrum of the conduction band $E^c_{\mathbf{K}}=E_0+[\hbar^2K^2/(2m_e)]$, the quantity $\xi(E^c_{\mathbf{K}}-\hbar\omega,\mathbf{K})$ can be represented in the form

$$\xi(E^c_{\mathbf{K}}-\hbar\omega,\mathbf{K})=[(\mu-2)x-\varepsilon][(\mu+2)x-\varepsilon+1]\ , \tag{A6}$$

where $\varepsilon=[(\hbar\omega-E_0)/\Delta_C]$. Using Eq. (12) we also obtain

$$E^v_{h\mathbf{K}}-E^v_{l\mathbf{K}}=2\Delta_C\sqrt{(1/2+2x)^2-3x\sin^2\vartheta}\ . \tag{A7}$$

Replacing $\sum_{\mathbf{K}}$ in (A1) and (A2) by $(2\pi)^{-2}\int_0^\infty dK\,K^2\int_{-1}^{1}d\cos\vartheta$, replacing $\int d\cos\vartheta$ with $\int d\cos^2\vartheta/(2\cos\vartheta)$, and using the δ function, we obtain $g(\omega)$ as

$$\begin{aligned}g(\omega)&=\frac{1}{4\pi^2}\int_0^\infty dK\,K^2\int d\cos^2\vartheta\frac{\sqrt{(2x+1/2)^2-3x\sin^2\vartheta}}{\Delta_C\sqrt{3x}}\\&\quad\times\delta(\xi+3x\sin^2\vartheta)\\&=\frac{1}{4\pi^2}\int_0^\infty dK\,K^2\frac{|\mu x+1/2-\varepsilon|}{\Delta_C\sqrt{3x(\xi+3x)}}\ .\end{aligned} \tag{A8}$$

There is a limit in the integration in Eq. (A8) resulting from the condition $\Delta(E)=0$. Since $0\le\cos^2\vartheta\le1$, a combination of Eqs. (A4) and (A5a) gives $-3x\le\xi(x)\le0$. As a consequence, we obtain $x_1\le x\le x_2$, or $x_3\le x\le x_4$ with $0\le x_1\le x_2\le x_3\le x_4$, where $\xi(x_1)=\xi(x_4)=0$, $\xi(x_2)=-3x_2$, and $\xi(x_3)=-3x_3$. Essentially the integration in Eq. (A8) can be divided into two parts:

$$g(\omega)=\frac{1}{4\pi^2\hbar^3}\left[\frac{2m_0}{\gamma_2}\right]^{3/2}\left[\frac{\Delta_C}{3}\right]^{1/2}\left[\int_{x_3}^{x_4}dx\frac{\mu x+1/2-\varepsilon}{\sqrt{(\xi+3x)}}-\int_{x_1}^{x_2}dx\frac{\mu x+1/2-\varepsilon}{\sqrt{(\xi+3x)}}\right]\ . \tag{A9}$$

Similarly, we obtain $\chi(\omega)$ as

$$\chi(\omega)=\frac{1}{4\pi^2\hbar^3}\left[\frac{2m_0}{\gamma_2}\right]^{3/2}\left[\frac{\Delta_C}{3}\right]^{1/2}\left[\int_{x_3}^{x_4}dx\frac{2x+1/2+\xi}{\sqrt{(\xi+3x)}}-\int_{x_1}^{x_2}dx\frac{2x+1/2+\xi}{\sqrt{(\xi+3x)}}\right]\ . \tag{A10}$$

The integrations in Eqs. (A9) and (A10) can be performed analytically and the results are

$$g(\omega)=\frac{\sqrt{\Delta_C}}{4\pi^2\hbar^3}\left[\frac{2m_0}{\gamma_2}\right]^{3/2}\left\{\frac{\mu}{\mu^2-4}\left[\left[\frac{\varepsilon}{\mu-2}\right]^{1/2}+\left[\frac{\varepsilon-1}{\mu+2}\right]^{1/2}\right]+\frac{\mu+4-8\varepsilon}{2\sqrt{3}(\mu^2-4)^{3/2}}Z(\omega)\right\}\ , \tag{A11}$$

$$\chi(\omega)=\frac{\sqrt{\Delta_C}}{4\pi^2\hbar^3}\left[\frac{2m_0}{\gamma_2}\right]^{3/2}\left\{\frac{1}{4(\mu^2-4)}\left[(4\varepsilon+\mu-3)\left[\frac{\varepsilon}{\mu-2}\right]^{1/2}+(4\varepsilon+\mu-1)\left[\frac{\varepsilon-1}{\mu+2}\right]^{1/2}\right]+\frac{16\varepsilon(\varepsilon-1)+4\mu\varepsilon-3\mu^2-2\mu+13}{8\sqrt{3}(\mu^2-4)^{3/2}}Z(\omega)\right\}\ , \tag{A12}$$

where

$$Z(\omega)=\ln\left|\frac{(1+\mu)^2-4\mu\varepsilon+16\varepsilon(\varepsilon-1)}{[4\varepsilon+\mu+1+2\sqrt{3\varepsilon(\mu+2)}][4\varepsilon+\mu-5-2\sqrt{3(\mu-2)(\varepsilon-1)}]}\right| . \tag{A13}$$

In the case $0<\varepsilon<1$, we have to use the real part of the result obtained from Eq. (A13).

*Permanent address: A. F. Ioffe Physical-Technical Institute, St. Petersburg, Russia.

[1]M. Kondow, H. Kakibayashi, and S. Minagawa, J. Cryst. Growth **88**, 291 (1988).
[2]A. Mascarenhas, S. Kurtz, A. Kibbler, and J. M. Olson, Phys. Rev. Lett. **63**, 2108 (1989).
[3]T. Suzuki and A. Gomyo, J. Cryst. Growth **111**, 353 (1991).
[4]S. Froyen, J. E. Bernard, R. Osorio, and A. Zunger, Phys. Scr. **T45**, 272 (1992).
[5]D. J. Friedman, S. R. Kurtz, A. E. Kibbler, K. A. Bertness, C. Kramer, R. Matson, D. J. Arent, and J. M. Olson, in *Evolution of Surface and Thin Film Microstructure,* edited by H. A. Atwater, E. Chason, M. H. Grabow, and M. G. Lagally, MRS Symposia Proceedings No. 280 (Materials Research Society, Boston, 1992), p. 493.
[6]R. G. Alonso, A. Mascarenhas, G. S. Horner, K. Sinha, J. Zhu, D. J. Friedman, K. A. Bertness, and J. M. Olson, Solid State Commun. **88**, 341 (1993).
[7]D. J. Friedman, A. E. Kibbler, and J. M. Olson, Appl. Phys. Lett. **59**, 2998 (1991).
[8]A. Gomyo, T. Suzuki, K. Kobayashi, S. Kawata, I. Hino, and T. Yuasa, Appl. Phys. Lett. **50**, 673 (1987).
[9]M. Kondow, H. Kakibayashi, S. Minagawa, Y. Inoue, T. Nishino, and Y. Hamakawa, J. Cryst. Growth **93**, 412 (1988).
[10]S. R. Kurtz, J. M. Olson, D. J. Arent, M. H. Bode, and K. A. Bertness, J. Appl. Phys. **75**, 5110 (1994).
[11]M. C. DeLong, P. C. Taylor, and J. M. Olson, Appl. Phys. Lett. **57**, 620 (1990).
[12]M. K. Lee, R. H. Horng, and L. C. Haung, J. Cryst. Growth **124**, 358 (1992).
[13]R. B. Capaz and B. Koiller, Phys. Rev. B **47**, 4044 (1993).
[14]D. B. Laks, S. H. Wei, and A. Zunger, Phys. Rev. Lett. **69**, 3766 (1992).
[15]T. Nishino, Y. Inoue, Y. Hamakawa, M. Kondow, and S. Minagawa, Appl. Phys. Lett. **53**, 583 (1988).
[16]S. R. Kurtz, J. M. Olson, and A. Kibbler, Sol. Cells **24**, 307 (1988).
[17]D. J. Mowbray, R. A. Hogg, M. S. Skolnick, M. C. Delong, S. R. Kurtz, and J. M. Olson, Phys. Rev. B **46**, 7232 (1992).
[18]M. C. Delong, D. J. Mowbray, R. A. Hogg, M. S. Skolnick, M. Hopkinson, J. P. R. David, P. C. Taylor, S. R. Kurtz, and J. M. Olson, J. Appl. Phys. **73**, 5163 (1993).
[19]G. S. Horner, A. Mascarenhas, S. Froyen, R. G. Alonso, K. Bertness, and J. M. Olson, Phys. Rev. B **47**, 4041 (1993).
[20]R. G. Alonso, A. Mascarenhas, S. Froyen, G. S. Horner, K. Bertness, and J. M. Olson, Solid State Commun. **85**, 1021 (1993).
[21]R. G. Alonso, A. Mascarenhas, G. S. Horner, K. A. Bertness, S. R. Kurtz, and J. M. Olson, Phys. Rev. B **48**, 11 833 (1993).
[22]D. E. Aspnes, J. P. Harbison, A. A. Studna, and L. T. Florez, J. Vac. Sci. Technol. A **6**, 1327 (1988).
[23]J. M. Luttinger, Phys. Rev. **102**, 1030 (1956).
[24]J. S. Luo, J. M. Olson, K. A. Bertness, M. E. Raikh, and E. V. Tsiper, J. Vac. Sci. Technol. B **12**, 2552 (1994).
[25]S. R. Kurtz, J. M. Olson, and A. Kibbler, Appl. Phys. Lett. **57**, 1922 (1990).
[26]T. Suzuki and A. Gomyo, J. Cryst. Growth **99**, 60 (1990).
[27]J. S. Luo and J. M. Olson (unpublished).
[28]D. J. Friedman, J. G. Zhu, A. E. Kibbler, J. M. Olson, and J. Moreland, Appl. Phys. Lett. **63**, 1774 (1993).
[29]S. R. Kurtz, J. Appl. Phys. **74**, 4130 (1993).
[30]C. Nozaki, Y. Ohba, H. Sugawara, S. Yasuami, and T. Nakanisi, J. Cryst. Growth **93**, 406 (1988).
[31]M. E. Raikh and E. V. Tsiper, Phys. Rev. B **49**, 2509 (1994).
[32]H. Lee, Ph.D. thesis, University of Illinois, Urbana, 1993.
[33]H. Kato, S. Adachi, H. Nakanishi, and K. Ohtsuka, Jpn. J. Appl. Phys. **33**, 186 (1994).
[34]P. Emanuelsson, M. Drechsler, D. M. Hofmann, B. K. Meyer, M. Moser, and F. Scholz, Appl. Phys. Lett. **64**, 2849 (1994).
[35]C. Wetzel, B. K. Meyer, and P. Omling, Phys. Rev. B **47**, 15 588 (1993).
[36]C. Hermann and C. Weisbuch, Phys. Rev. B **15**, 823 (1977).